# 1 Abstract

We use the radial velocity of NGC 604 obtained with the ISIS instrument (long slit spectroscopy) to study the results obtained from the second order structure function. The $H_\alpha$ emission line is used for being the brightest among the observed lines. To see how the structure function is affected, we change the spatial size (Test 1, Test 4) and the PDF (Test 2, Test 3) of the velocity sample. We analyzed not only its form, also the two main parameters obtained with it, the correlation length, $l_0$, and the slope, $m_{2D}$. Despite a dependency on the results and the selected samples, the indices obtained and correlations lengths still hold some information on the physics of the region since there is a clear range in the data. For $m_{2D}$ the results encompass 0.9 to 1.8 and for $l_0$, 30 to 10 pc.

# 2 Intro

The structure function has been used as a diagnostic tool to evidence the presence of turbulence in HII regions and giants extragalactic HII regions (GEHRs) (Von Hoerner, 1951; Münch, 1958; Medina-Tanco et al., 1997; Lagrois and Joncas, 2009; Melnick et al., 2019). Multiple investigations have proven is usefulness (Castaneda, 1988; Lagrois and Joncas, 2011) as many others have suggested better methods (Medina et al., 2014; Arthur et al., 2016) for studying the underlying velocity fluctuations in the ionized gas. Interpreting the structure function of the ISIS observations have been quite a challenge. Since there are few points (600, many data is discarded), the results obtained by statistical tools need to be examine carefully so we do not arrive to wrong conclusions. Here the importance of knowing what drives the structure function form and what can be attributed to foreign artifacts.

Since the nature of giant HII region is quite a challenge itself, the why it has been measure in these objects (and their galactic counterparts), close values related to turbulent theory still remains a question without answer and we can expect that that none will arrive soon. So, our understanding on the limitations of our methods and observations will be necessary to know at what extent our results are valid in the context of theory. As the main goal is to understand how the physics on the GEHRs play a role on turbulence and its related problems, we must first understand what are our methods telling us and how these interpretations are related to what is happening in the region.

For this, we aim to study how the main parameters obtained by a second order structure function are changing when the analyzed sample has been spatially and statistically reduced. For this we apply what we called 'Test 1' where the complete sample of the region is first used and the is spatially reduced. For the 'Test 2' we start eliminating small brightness values till we arrive to the brightest part of NGC 604. For Test 3 me start reducing the velocity sample starting for its extreme values. Finally in Test 4 we analyzed 1/3 of our observations and move the window across all the original area.

# 3 Methods

## 3.1 Astronomical observations

The archival data used in this work were retrieved from the La Palma archive[1] and reduced again by Pérez-Oregón (2013) using the IRAF (National Optical Astronomy Observatories, 1999) astronomical software. The data used in this work was obtained with the ISIS spectrograph in the 4.2-m William Herschel Telescope of del Roque de los Muchachos Observatory (ORM) in La Palma, Spain. The ISIS observations have been used by Maíz-Apellániz et al. (2004) and Tenorio-Tagle et al. (2000). Maíz-Apellániz et al. (2004) provides the details of the observational setup. The spectra were obtained using a position angle of 90° and the slit width was 1". The spectra for the red arm has a range of 6390 and 6849 Å. The slit has a length of 200" and for NGC 604 (Fig. 1[2]) ten positions were observed with an exposure time of 1000 s for each slit position.

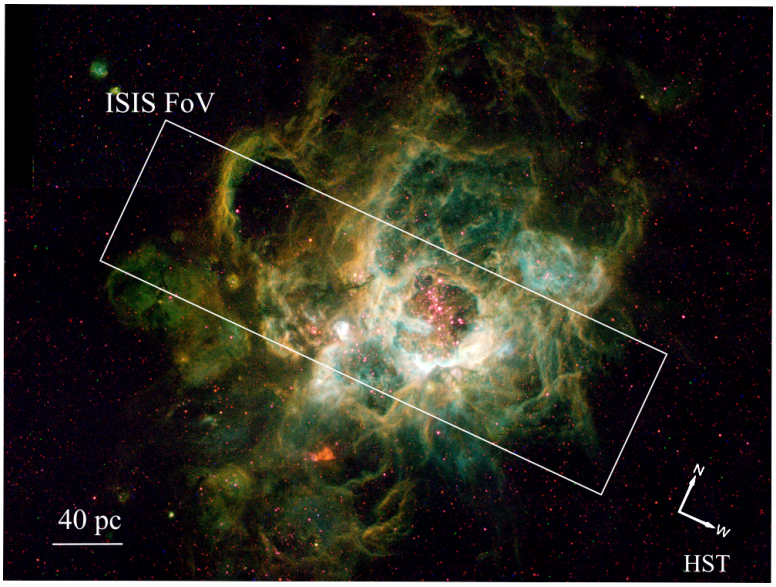


Figure 1: Image of NGC 604 captured with the Hubble Space Telescope with the observations cover by ISIS (Credit: Hui Yang (University of Illinois) and NASA/ESA).

[1] http://casu.ast.cam.ac.uk/casuadc/ingarch
[2] https://esahubble.org/images/opo9627c/

### 3.2 Tests

Equation 1 is applied to different velocity samples considering different conditions of the original data, see Fig. 2.

$$S_2(\boldsymbol{l}) = \frac{\sum[V_r(\boldsymbol{x}+\boldsymbol{l}) - V_r(\boldsymbol{x})]^2}{N(\boldsymbol{l})} \quad (1)$$

For Test 1 we are changing the spatial area of the sample that is analyzed with the structure function. In Fig. 3 we show the different zones (1-4). Also there is a zone (5) which corresponds to the brightest area of NGC 604 and some identified shells (Sabalisck et al., 1995; Yang et al., 1996; Tüllmann et al., 2008).

For Test 2 we start getting rid of values with low emission; this limitation takes into account that ISIS observations are more reliable in high emission pixels. Figures 4 shows the different emissions zones consider in Test 2, where the change consider values on A.D.U. $> 0$ , 150, 1 500 and 3 000; this samples are named '0' (same test 1), '6', '7' and '8'.

For Test 3 we eliminate the extreme values of the radial velocity sample. Figure 5 show how the velocity maps are changing. The velocity samples are named '9' to '11'.

In Test 4 we chose a window of 108 pc and move it 20 pc in west direction starting from the far left side. In this case the samples are named from '12' to '22'.

Figure 7 shows the histogram of the different samples.

We are using as main parameters the value of the slope, $m_{2D}$, obtained with a fit using S(l)=[2-C(l)] where C(l)=1/[1-(l/$l_0$)$^{m_{2D}}$] and $l_0$ is the correlation length, the $l$ value where S(l)=$\sigma^2$ (Scalo, 1984; Arthur et al., 2016).

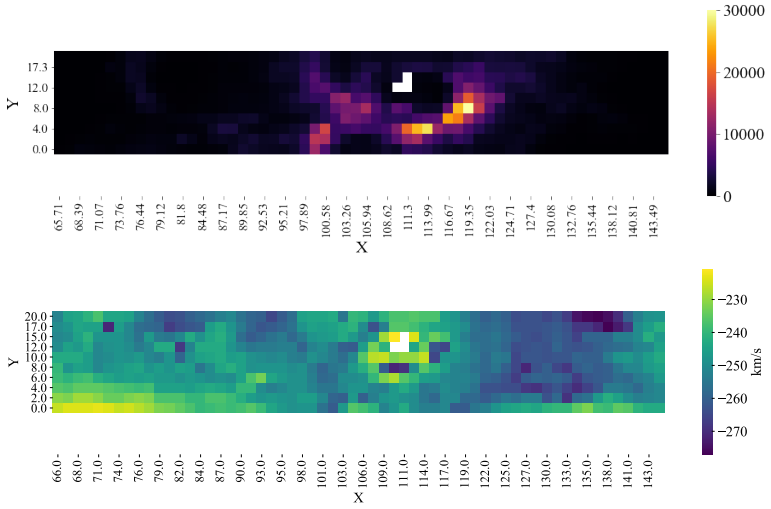


Figure 2: Bidimensional maps of emission flux and heliocentric radial velocity of NGC 604 (Sample '0').

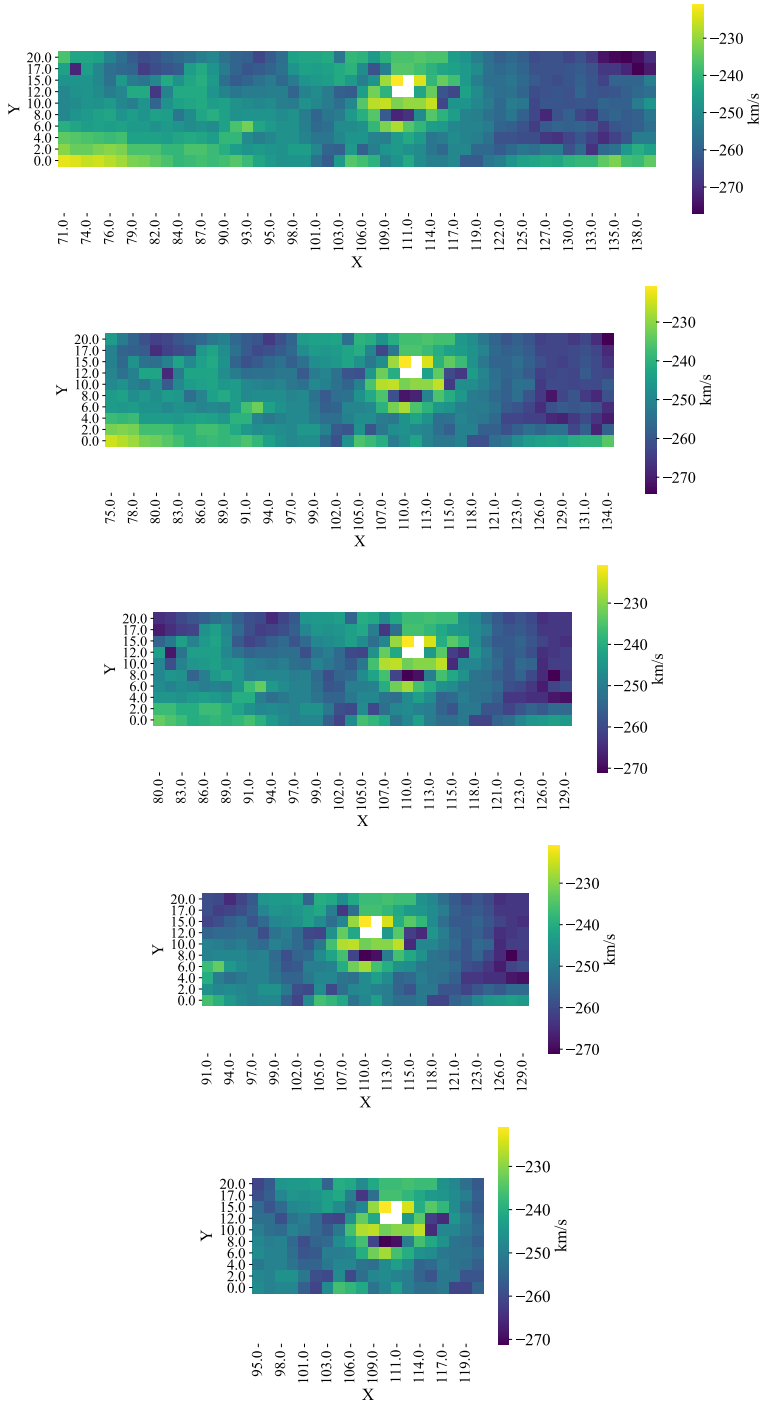


Figure 3: Test 1 samples: '1' to '5' starting from above.

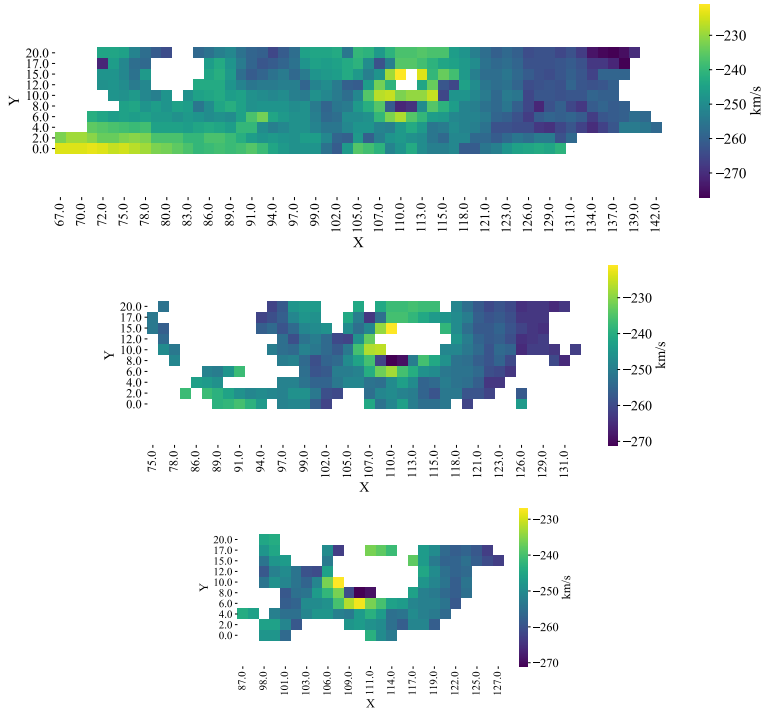


Figure 4: Test 2 samples: ’6’ to ’8’ starting from above.

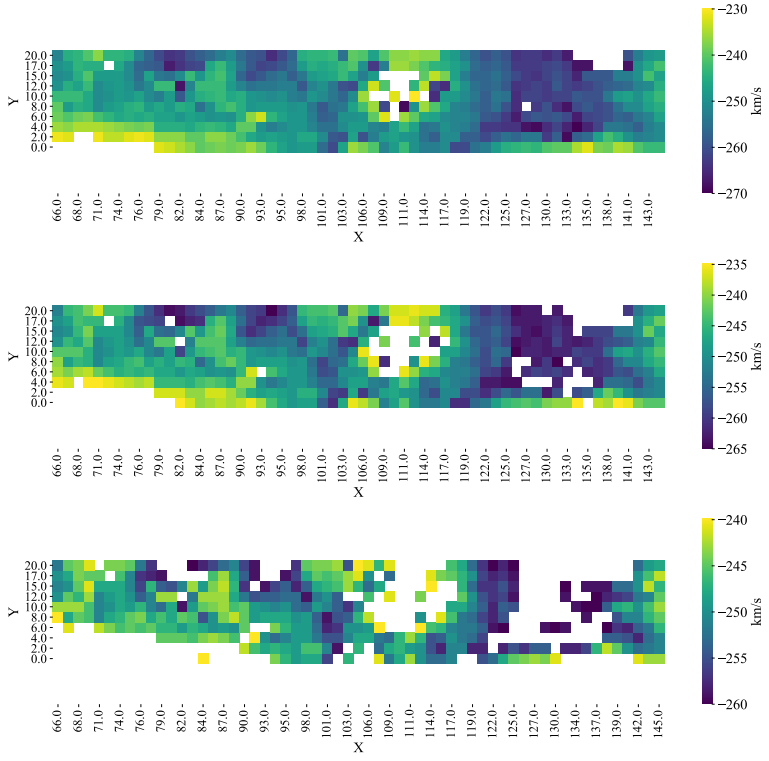


Figure 5: Test 3 samples: ’9’ to ’11’ starting from above.

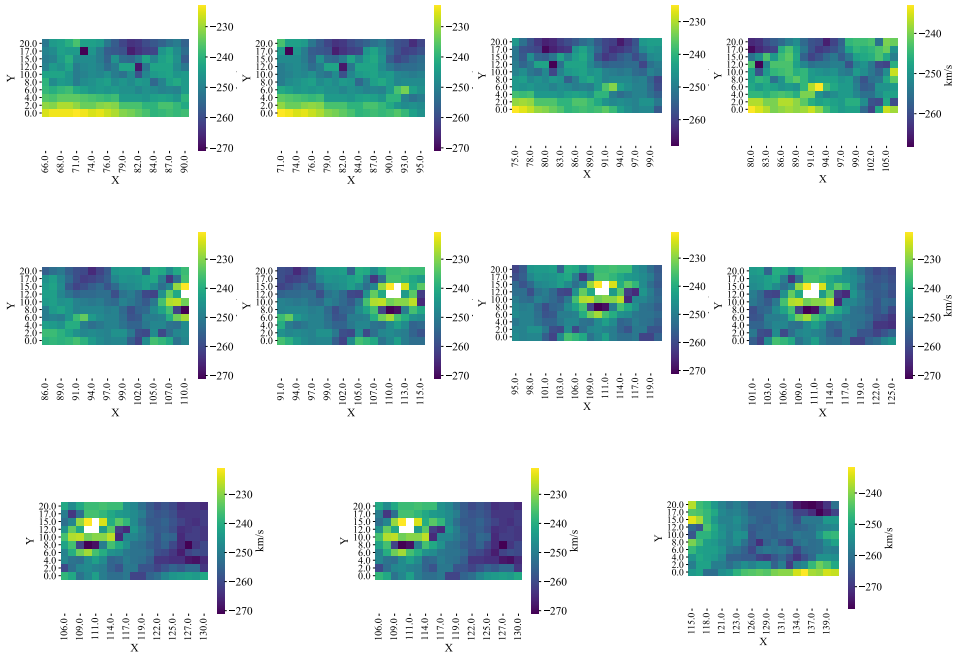

Figure 6: Test 3 samples: ’12’ to ’22’ starting from above left.

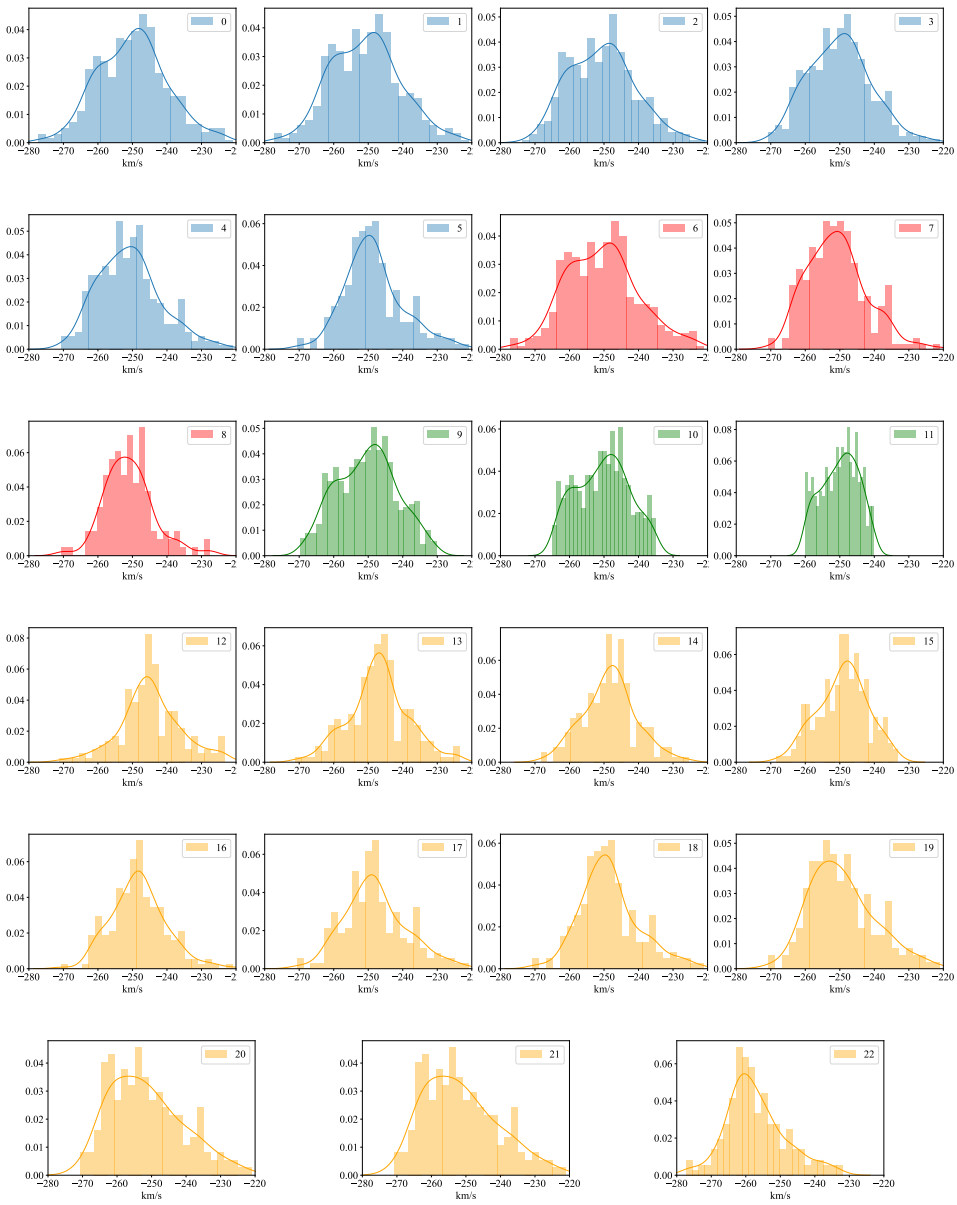


Figure 7: Histograms of the different samples.

# 4 Results

Table 1 shows the results of the fit of the structure function for all samples and Figure 8 shows the structure function of each sample. For all these results, the first point which corresponds to the smallest scales is not consider for the the fit to find the power-law index. The reason is that for scales below 5 pc the seeing is influencing our observations.

Sample '0', which serves as reference because of its sample size, has a value of 1.1 for the index between 8 pc and the correlation length 25 pc. It´s $\sigma$ is 10.05 km/s with a $L_c/l_0$ of 13. The structure function goes up until a value of 80 pc. Above the 100 pc scale the structure function goes into a 'periodic' behavior with a 'frequency' of 100 pc with two complete 'cycles' until 300 pc scales.

For Test 1, the value $m_{2D}$ stays around the reference value going stepper for sample '3' and '4' to a value a of 1.2. For this sample there is a jump in the correlation length going from 23 pc for sample '2' to 14 pc for sample '3' and 12 pc for sample '4'. The $L_c/l_0$ ratio has a minimum of 10 and a maximum of 14. The periodic behavior still is presents and only shows a diminution to 1.5 cycles, corresponding to the reduction in the sample box. This periodic behavior is completely eliminated in sample '5', where the structure function falls steeply, but there isn't enough points for a fit. The value of $\sigma$ also shows a decrease in its value, going from 10.05 to 8.59 km/s.

In Test 2, the results for the sample '0' and '6' are quite similar mainly because the sample are much alike. Sample '6' considers emission values above 150 A.D.U. The number of masked pixels is 117 and does not have a significant weight on the structure function. The index values goes from 1.1 to 1.0, $l_0$ increase to 31 pc and related with this we have a increase in $\sigma$ of 0.34 kms/s, giving us a value of 10.39 kms/s for sample '6'. There is a tendency for the structure function values to rise, going steeper with larger scale. There is is a 'bump' in the structure function at scales of 100 pc.

From Fig. 7 we can see that sample '0' (blue) and '6' (red) show a double peak behavior, previously reported for this GEHR (Rosa and D'Odorico, 1982; Yang et al., 1996; Tenorio-Tagle et al., 2000). This come from the zone between X, 107-118, and Y, 10 and 15. If we mask this zone we can get rid of this behavior, as samples '7' and '8' reveal; what it remains has been called, *kinematic core* because of its 'well' behaved Gaussian fit (Sabalisck et al., 1995; Muñoz-Tuñon et al., 1996).

Sample '7' show the highest $m_{2D}$ value (even considering Test 1) of 1.8. The spatial length of the analyzed zone is 230 pc and the correlation length is 14 pc giving a ration of 16. Here we notice that the correlation length is half the sample '6'. The $\sigma$ decrease to 8.55 km/s with comparison to sample '0'. Sample '8' presents the problem that just a single point is behind the correlation length and this can not be used because of seeing, so no fit can be done. The $l_0$ value is 10 pc with a $\sigma$ of 7.28 km/s, the lowest of all samples. For Test 2 the tendency of the ratio $L_c/l_0$ is to increase towards the brightest samples. The 'periodic' tendency at large scales still is present for samples '7' and '8'

For Test 3, there is no clear tendency in the parameters, thought the correlation length drops from 23 to 14 pc from samples '9' and '10' to '11'. There is a reduction in the value of $\sigma$ for each sample, and sample '11' has the highest index of 1.8 with the highest $L_c/l_0$ ratio of 23. Fig. 7 shows the histograms (green) for each sample and we can see that the double peak behavior is diminished but still appears in all the samples. The periodic behavior at larges scale still is present. For samples '9' and '10' the form is quite similar to sample '0' but for sample '11' there is an increase in the 'frequency' of the oscillation.

For Test 4, there is the interesting fact that despite the length of the box staying constant there is a variation in the indices and correlation lengths. The lowest value is 0.9 for a region in the west (sample '21') with a $l_0$ of 26 pc and a ratio of 4. While the higher value is 1.7 for $m_{2D}$ and a $l_0$ of 15 pc and a ratio of 7 for sample '15' which is located in the east part of the region. Samples '16' to '19' where unable to provide a good a fit. This samples consider and expanding shell, mentioned earlier (Test 2), but despite also having the same kinematical zone samples '21' and '22' where able to provide a reasonable good fit. There is some variation in the $\sigma$ and the range goes from 7 to 10 km/s. Despite having a 3 km/s difference it is worth noting that this kind of reflect some homogeneity in the value of $\sigma$ across the region. For Test 4 samples, at larges scales the periodic pattern is eliminated. Either some structure functions tends to keep the behavior of going up, other presents a drastic decrements in the structure function values.

Table 1: Main results.

| Test | Name | Condition | Length | $m_{2D}$ | $l_0$ [pc] | $\sigma$ [km/s] | $L_c/l_0$ | No. points |
|---|---|---|---|---|---|---|---|---|
| Control | 0 | 65-145 | 320 | 1.1 | 25 | 10.05 | 13 | 597 |
| 1 | 1 | 70-140 | 280 | 1.0 | 25 | 10.08 | 11 | 517 |
| 1 | 2 | 75-135 | 240 | 0.9 | 23 | 9.55 | 10 | 447 |
| 1 | 3 | 80-130 | 200 | 1.2 | 14 | 9.98 | 14 | 367 |
| 1 | 4 | 90-130 | 160 | 1.2 | 12 | 9.15 | 11 | 287 |
| 1 | 5 | 95-121 | 104 | - | 8 | 8.59 | 13 | 197 |
| 2 | 6 | >150 | 320 | 1 | 32 | 10.39 | 10 | 480 |
| 2 | 7 | >1 500 | 228 | 1.8 | 14 | 8.55 | 16 | 239 |
| 2 | 8 | >3 000 | 160 | - | 10 | 7.28 | 16 | 124 |
| 3 | 9 | -270,-230 | 320 | 1.2 | 23 | 8.68 | 14 | 566 |
| 3 | 10 | -265,-235 | 320 | 1.3 | 23 | 7.6 | 14 | 525 |
| 3 | 11 | -260,-240 | 320 | 1.8 | 14 | 5.31 | 23 | 401 |
| 4 | 12 | 65-91 | 104 | 1.5 | 25 | 8.84 | 4 | 190 |
| 4 | 13 | 70-96 | 104 | 1.5 | 25 | 8.72 | 4 | 190 |
| 4 | 14 | 75-101 | 104 | 1.5 | 22 | 7.76 | 5 | 200 |
| 4 | 15 | 80-106 | 104 | 1.7 | 15 | 7.17 | 7 | 200 |
| 4 | 16 | 85-111 | 104 | - | 10 | 7.92 | 10 | 189 |
| 4 | 17 | 90-116 | 104 | - | 8 | 9 | 13 | 187 |
| 4 | 18 | 95-121 | 104 | - | 8 | 8.59 | 13 | 197 |
| 4 | 19 | 100-126 | 104 | - | 9 | 9.38 | 12 | 187 |
| 4 | 20 | 105-131 | 104 | 1.2 | 13 | 10.59 | 8 | 187 |
| 4 | 21 | 110-136 | 104 | 0.9 | 26 | 9.94 | 4 | 180 |
| 4 | 22 | 115-141 | 104 | 1.5 | 19 | 8.61 | 5 | 200 |

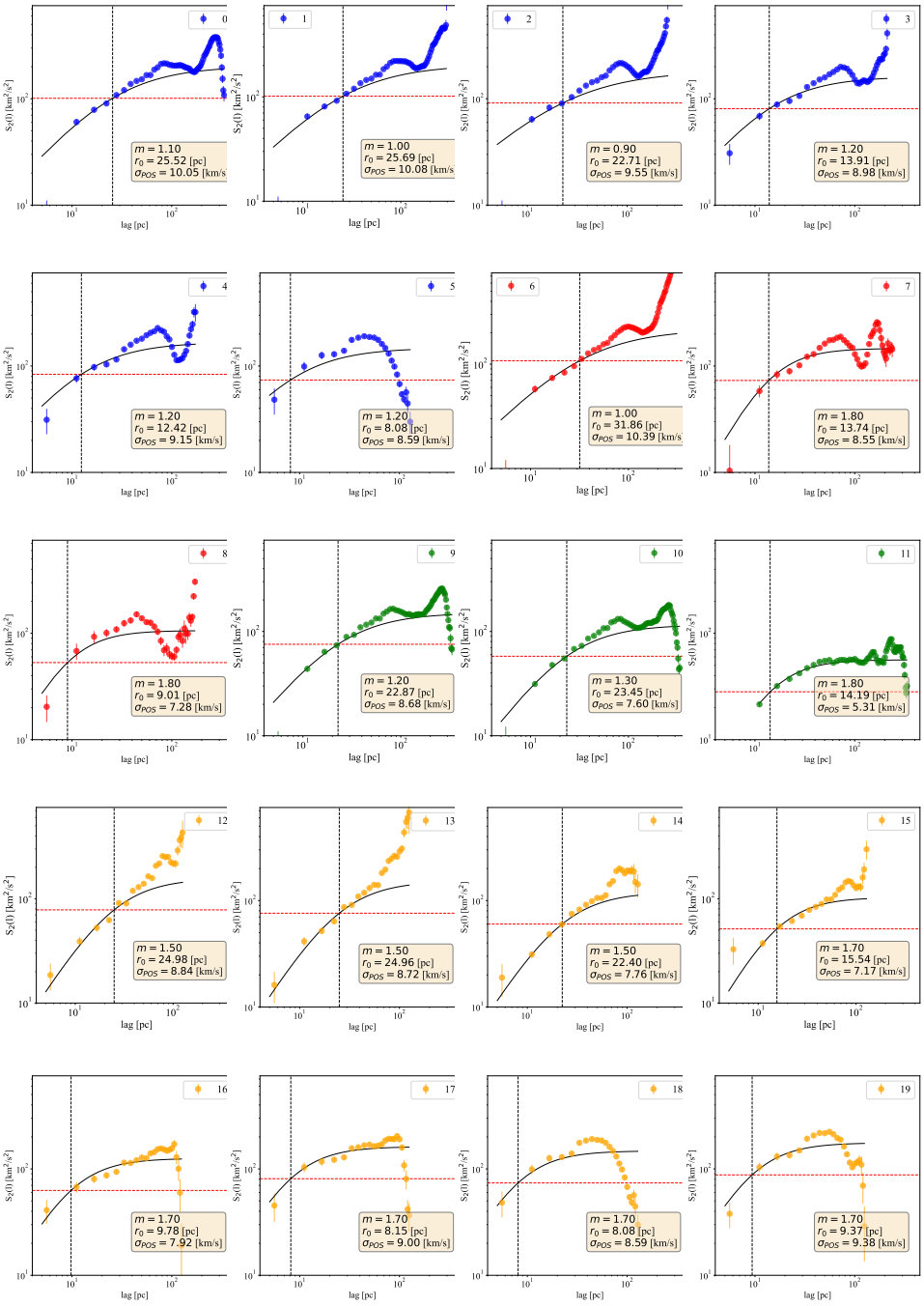


Figure 8: Structure Function. Samples '0'-'19'.

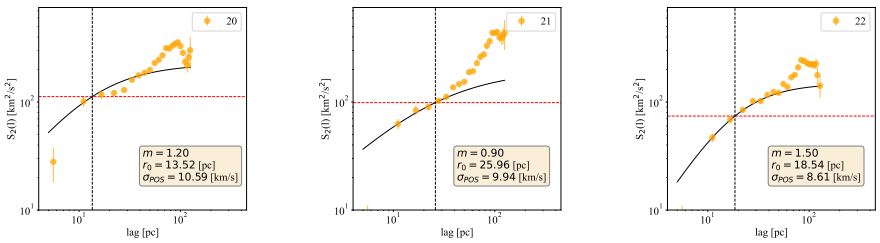


Figure 9: Structure Function. Samples '20'-'22'

# 5 Discussion

The large range of values of $m_{2D}$ between samples shows that this parameter is not reliable as a single diagnosis for the turbulent state of the ionized gas, the same goes for $l_0$. Despite showing a strong dependency on the sample these values still hold information that can be used. The index goes to a maximum of 1.8 at a length of 233 pc and considers the brightest part of the region. In this case the observations are not just centered in the bright emission zone, they cover some extent of the outside region, which can give us insight is something is going on through all the nebula that can be related. It has been mentioned that hot gas that has escaped the hot supper bubbles, consequences of the stellar winds, is flowing 'freely' inside the region (Tüllmann et al., 2008).

The consistency of the periodic behavior at larger scales can be consider as a real 'motion' since it has proven to be omnipresent in our results. The oscillation in the range of 100 pc should also mark some limit where energy injection can be happening. For this regions it have been determined gradients in the east west direction that have been attributed to the rotation of the region (Hippelein and Fried, 1984).

The maximum and minimum values of $l_0$ may be used to determined some limits where the energy injection is happening; this if we consider the classic Kolmogorov cascade model. The scales 28 to 10 pc can be attributed to many things, among others, they correspond to the radius of the expanding shells present in NGC 604 (Yang et al., 1996). Though, there is no clear correlation, far by a causation it worth pointing it out. We already mentioned that samples 0 and 10 show a double peak behavior. The elimination of this to a more Gaussian fit does not influence in a considerable way the results. Which raise the question: At what extent this shells play a role in the structure function?

However, the power-law indices show a clear tendency between 1.2 and 1.8 which far from been concluding also are telling something relevant; that we can limit our astronomical observations to this range of values.

If we compute the $m_{3D}$ index through projection smoothing and a sheet-like distribution limits it is possible to use; $m_{2D}$ - 1 $< m_{3D} < m_{2D}$, having 0.8 $< m_{3D} <$ 1.2, been $m_{3D}$ above the Kolmogorv prediction. This shouldn't be a surprise since physical conditions in GEHRs are different from the homogeneous and incompressible ideal model, as many authors have mentioned (Münch, 1958; Castaneda, 1988; Lagrois and Joncas, 2011; Arthur et al., 2016).

As for the $L_c/l_0$ ratio can be seen how much smaller is in tendency the correlation length related to the sample area. The diminution in $l_0$ is correlated with the $\sigma$, since lower $\sigma$ impose smaller correlation lengths. The issue with this change in $\sigma$ is that clearly shows that there isn't statistically homogeneity in our data.

Also, the numbers of points have show that there is a limit where the fit can be done to the structure function. Samples '9', 'a' and '12', which respectively have 260, 200 and 124 where unable to give reliable information.

# 6 Conclusions

The variation on the $m_{2D}$ indices and the correlation length can be attributed to the variation in the analyzed samples. Since no two samples where the same, our results show dependency on the velocity field and the structure function form. The $m_{2D}$ index goes from 1.2, for a sample with length 318 pc that considers all the points, to a value of 1.8 for a 233 pc length for a sample who considers only a bright region. Since the $\sigma$ of the sample is getting smaller, the same is happening to the correlation length, $l_0$. This breaks possibility of determining the scale where energy injection is happening using this method, thought is seems rarely that this is the case on this or any other GEHR. Also, there is nothing conclusive regards if stellar winds, champagne flows, or other kinematic assumptions, are registered through the structure function. The change in the form and in the two main diagnostic parameters make this method no as reliable as one would have wanted, but it impose some constraints where we can expect other results for GEHR.

ISIS long-slit spectroscopic observations have been proven useful in obtaining the structure function for NGC 604. The second order structure form has a dependency on its input data, but this does not weight enough to overlook the information that it can give, but also is recommendable that others methods are used in determining turbulent information of a GEHR.

# References


Arthur, S., Medina, S., and Henney, W. (2016). Turbulence in the ionized gas of the Orion nebula. *MNRAS*, 463(3):2864–2884.

Castaneda, H. O. (1988). The Velocity Structure and Turbulence at the Center of the Orion Nebula. , 67:93.

Hippelein, H. and Fried, J. (1984). Turbulent gas motions in giant H II regions. I-The case of NGC 604. *A&A*, 141:49–55.

Lagrois, D. and Joncas, G. (2009). A Multi-ionic Kinematic Investigation of NGC 595, a Giant Extragalactic H II Region in M33. , 700(2):1847.

Lagrois, D. and Joncas, G. (2011). Extraction of homogeneous turbulent motions in the ionized interstellar medium: application to the NGC 595 nebula. , 413(2):721–740.

Maíz-Apellániz, J., Pérez, E., and Mas-Hesse, J. (2004). NGC 604, the Scaled OB Association (SOBA) Prototype. I. Spatial Distribution of the Different Gas Phases and Attenuation by Dust. *AJ*, 128(3):1196.

Medina, S.-N., Arthur, S., Henney, W., Mellema, G., and Gazol, A. (2014). Turbulence in simulated HII regions. *MNRAS*, 445(2):1797–1819.

Medina-Tanco, G., Sabalisck, N., Jatenco-Pereira, V., and Opher, R. (1997). Structure, velocity fielda, and turbulence in NGC 604. *AJ*, 487(1):163.

Melnick, J., Terlevich, R., Tenorio-Tagle, G., Telles, E., and Terlevich, E. (2019). On the nature of supersonic turbulence in Giant HII Regions. *arXiv e-prints*, page arXiv:1912.03543.

Muñoz-Tuñon, C. Tenorio-Tagle, G., Castañeda, H., and Terlevich, R. (1996). Supersonic line broadening and the gas dynamical evolution of giant H II regions. *AJ*, 112:1636.

Münch, G. (1958). Internal motions in the orion nebula. *Reviews of Modern Physics*, 30(3):1035.

National Optical Astronomy Observatories (1999). IRAF: Image Reduction and Analysis Facility.

Pérez-Oregón, J. (2013). Propiedades generals de algunas regiones HII. Master's thesis, IPN.

Rosa, M. and D'Odorico, S. (1982). Wolf-Rayet stars in extragalactic H II regions. II-NGC604-A giant H II region dominated by many Wolf-Rayet stars. *A& A*, 108:339–343.

Sabalisck, N. S., Tenorio-Tagle, G., Castaneda, H. O., and Munoz-Tunon, C. (1995). On the supersonic turbulence of NGC 604. *ApJ*, 444:200–206.

Scalo, J. (1984). Turbulent velocity structure in interstellar clouds. *The Astrophysical Journal*, 277:556–561.

Tenorio-Tagle, G., Muñoz-Tuñón, C., Pérez, E., Maíz-Apellániz, J., and Medina-Tanco, G. (2000). On the ongoing multiple Blowout in NGC 604. , 541(2):720.

Tüllmann, R., Gaetz, T., Plucinsky, P., Long, K., Hughes, J., Blair, W., Winkler, P., Pannuti, T., and Breitschwerdt, D.and Ghavamian, P. (2008). Chandra ACIS Survey of M33 (ChASeM33): A first look. *AJ*, 685(2):919.

Von Hoerner, S. (1951). Eine methode zur untersuchung der turbulenz der interstellaren materie. mit 10 textabbildungen. *Zeitschrift fur Astrophysik*, 30:17.

Yang, H., Chu, Y., Skillman, E., and Terlevich, R. (1996). The violent interstellar medium of NGC 604. *AJ*, 112:146.